

Direct and accurate patterning of plasmonic nanostructures with ultrasmall gaps

Cite this: *Nanoscale*, 2013, 5, 4309

Guangyuan Si,^{†a} Yanhui Zhao,^{†b} Jiangtao Lv,^a Fengwen Wang,^a Hailong Liu,^c Jinghua Teng^{*d} and Yan Jun Liu^{*d}

We report an improved method to directly and accurately fabricate plasmonic nanostructures with ultrasmall gaps. The fabrication is based on high-resolution focused ion beam milling with closely packed nanoring patterns. With fine and precise adjustment of the ion beam, elegant plasmonic nanostructures with ultrasmall dimensions down to 10 nm are achieved. We also show that the gap dimensions have a strong effect on the optical reflectance and transmittance of the plasmonic nanostructures. Measured results show reasonable agreement with finite-difference time-domain calculations. Our approach could find promising applications in plasmon-assisted sensing and surface-enhanced spectroscopy.

Received 5th February 2013

Accepted 7th March 2013

DOI: 10.1039/c3nr00655g

www.rsc.org/nanoscale

Introduction

Plasmonic nanostructures have gained extensive attention and found great potential in nanophotonic applications. Since the experimental demonstration of extraordinary optical transmission¹ and theoretical prediction of the perfect lens,² researchers have witnessed an explosion of investigations on invisibility cloaking,^{3,4} superlensing,^{5,6} optical waveguiding,^{7,8} and biosensing.^{9,10} Numerous approaches have been realized using a variety of geometries, including nanoshells,^{11,12} nanorings,^{13–18} nanorice,¹⁹ nanodisks^{20,21} and nanogratings.²² All these achievements take advantage of the highly shape-dependent properties of plasmonic nanostructures, because electromagnetic waves can be coupled to collective electron oscillations (*i.e.*, surface plasmons) on metal–dielectric interfaces, existing as either propagating or localized modes. These plasmon modes can be supported by various structures at broad scales and shapes, enabling huge potential in realizing plasmonic devices with desired optical functions, for instance, switches,²³ modulators,²⁴ sensors,²⁵ and color filters.^{16,17} Among all these plasmonic devices, regimes with ultrasmall gaps are of particular importance due to the fundamental physical interest of confining light to deep subwavelength dimensions and their great potential in sensing and switching. In addition, sharp

resonances can provide high quality factors and therefore give rise to high sensitivities, opening up new opportunities for bio/chemical-sensing.

Ultrasmall plasmonic gaps can strongly localize electric fields, hence significantly enhancing photon–plasmon coupling/conversion efficiency. Dramatic field enhancement can be observed in ultrasmall gaps.^{26–34} However, it is extremely challenging to achieve ultrasmall gap features with well-defined dimensions and uniformity. To date, the most frequently used top-down fabrication methods for plasmonic devices are electron-beam lithography (EBL) and focused ion beam (FIB) techniques. EBL is capable of defining diverse patterns down to nanoscale dimensions in polymer resists. It is normally combined with stripping (lift-off) or etching (dry etching and wet etching) to transfer patterns. For the lift-off method, it is cumbersome to make the fabrication process effective when the features go down to tens of nanometers, especially for dense arrays, because resists are difficult to strip away. With wet etching techniques, it is difficult to control the processes since etching rates are quite sensitive to chemical etchant concentration and other parameters like temperature and pressure. Another common problem of wet chemical etching is rough sidewalls due to nonuniform etching rates. In contrast, dry etching can produce smooth sidewalls and improve etching profiles considerably. However, thin resist thickness and selectivity issues limit the dry etching process and make it only applicable to non-deep etching.

Since ions are remarkably larger than electrons and they can carry more momentum than electrons after acceleration under a certain voltage, they can strike a target with greater energy density at relatively short wavelengths to directly define patterns in hard materials. Thus, the application of an electron-beam stays primarily in the realm of imaging while ions are expected to produce and manufacture sharp and high resolution features under optimized conditions. Using the FIB technique, one can

^aCollege of Information Science and Engineering, Northeastern University, Shenyang 110004, China

^bDepartment of Engineering Science and Mechanics, The Pennsylvania State University, University Park, PA 16802, USA

^cMeasurement Technology & Instrumentation Key Lab of Hebei Province, Institute of Electrical Engineering, Yanshan University, Hebei, 066004, China

^dInstitute of Materials Research and Engineering, Agency for Science, Technology, and Research (A*STAR), 3 Research Link, Singapore 117602. E-mail: liuy@imre.a-star.edu.sg; jh-teng@imre.a-star.edu.sg

[†] These authors contributed equally to this work.

directly mill patterns with features down to the nanoscale without using masks. In addition, this maskless lithography is almost non-selective to all materials. Here, we present an elegant way to fabricate ultrasmall gaps in optically thick metal films. Features down to 10 nm are fabricated using an improved FIB patterning method. We also show that the gap dimensions have a strong effect on the optical reflectance and transmittance of the plasmonic nanostructures. Fine tuning of the plasmon resonance through geometric control is experimentally demonstrated and theoretically verified.

Fabrication of ultrasmall gaps

An optically thick (160 nm) gold film was deposited on quartz substrates with 3 nm titanium as the adhesion layer using electron-beam evaporation. To minimize the roughness introduced by metal film deposition, low evaporation rates were applied (less than 0.05 nm s^{-1} average deposition rate). Both titanium and gold films were sequentially deposited on quartz substrates without breaking the vacuum in the evaporator chamber at a base pressure of about 2×10^{-7} mbar. Using FIB, dense plasmonic arrays were directly milled based on pre-defined closely packed nanoring patterns, as shown in Fig. 1(a). To minimize redeposition effects, all patterns were milled in parallel. An 11 pA probe current (corresponding to 15 nm spot diameter) was selected with 30 kV acceleration voltage to mill

the ring patterns. The total milling time for a 13×12 ring array was approximately 7 minutes. Previously, we have shown that ring shapes are much more resistant to the tapering effect than standard cylindrical holes during pattern definition using FIB in dielectric materials (lithium niobate, for instance).³⁵ In this work, by closely packing coaxial ring-like structures, we can remove the gold materials within the regimes between coaxial structures, leaving dense plasmonic arrays with controllable lattice shape, as illustrated in Fig. 1(a). More importantly, compared to the milling of circular apertures, more beam energy can be concentrated in the ring area, hence remarkably reducing the energy dissipation and total etching time during the FIB process and enabling ultrasmall features and a large etching depth simultaneously. Using such an improved FIB patterning method, one can simply fabricate metallic nanorods with large aspect ratios. Moreover, one can easily control the geometry by varying the inner and outer radii of individual rods and changing the distance between the rods to accurately control the overlapping areas. Therefore, the entire process is highly accurate and monolithic. Fig. 1(b) shows the typical scanning electron microscope (SEM) image of the plasmonic array under investigation in this work which consists of circle- and diamond-shaped lattices. Precise control of the lattice shape and edge-to-edge separation (ETES) can be realized. Here, ETES is defined as $\text{ETES} = r_2 - r_1$, where r_2 and r_1 are the outer and inner radii of the ring aperture for FIB milling. It is worth mentioning that for all the milled samples discussed in this work, the gold films were milled through completely in order to exclude the etching depth effect on the optical responses.

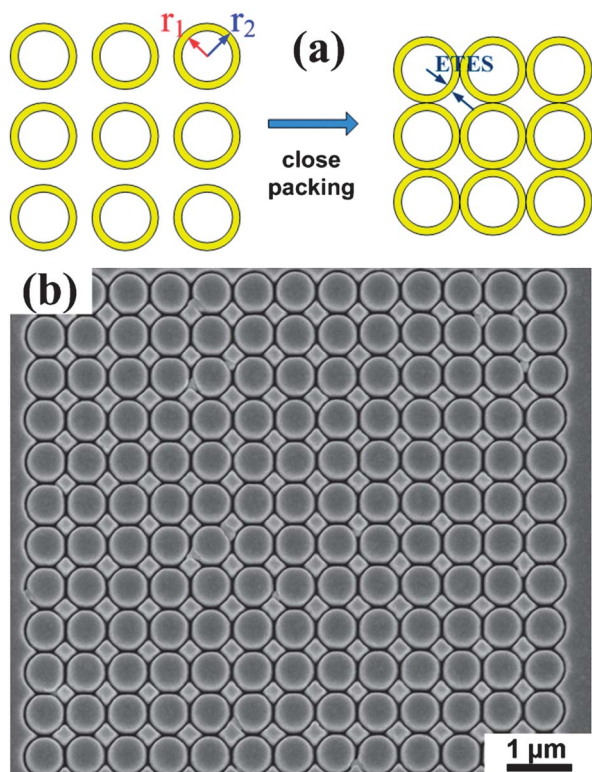


Fig. 1 (a) Schematic diagram of the FIB lithography method for nanorod fabrication based on nanoring patterning. (b) SEM image (overview) of the typical design proposed in this study formed by diamond-circle shaped lattices ($\sim 8 \times 8 \mu\text{m}^2$ area).

Simulations and optical characterization

Finite-difference time-domain (FDTD) calculations (Lumerical)³⁶ were carried out to theoretically explore the properties of plasmonic arrays with ultrasmall ETES. The dispersion model of gold was based on Johnson and Christy³⁷ in the material library of the software. Simulation regions were set to include four complete lattices to observe the coupling effect among the ultrasmall gaps in adjacent lattices with periodical boundary conditions applied on the two dimensional models to simulate the case of periodical arrays in a large scale. Incident wavelength was selected to cover the range from 300 nm to 1300 nm, corresponding to the measured bands of the microspectrometer.

The optical measurements were performed using a microspectrometer (CRAIC QDI 2010™) with a 75 W broadband xenon source. Transmittance and reflectance measurements were normalized to a bare quartz substrate and an aluminum mirror, respectively. The probe light beam was focused onto the sample surface to have a detecting area of $7.1 \times 7.1 \mu\text{m}^2$ using a $36\times$ objective lens combined with a variable aperture.

Results and discussion

Fig. 2 demonstrates the gradually decreased ETES (90 nm (left) to 10 nm (right) with a fixed outer radius $r_2 = 330$ nm and varied inner radii $r_1 = 240$ nm (left) to 320 nm (right) in 20 nm step-size increments), indicating a precise and programmable

control of FIB on fabricating such pre-designed structures. Fig. 3 plots the measured reflectance and transmittance of the corresponding nanostructures shown in Fig. 2. Interestingly, a distinct sharp peak (indicated by the brown arrow in Fig. 3(a)) appears in the reflectance spectra with gradually decreased ETES, which is similar to an observation on electromagnetically induced reflectance (EIR) termed by Liu and co-workers.³⁸ It is shown in Fig. 3(a) that only broad resonances (between 500 nm and 600 nm) can be observed when the ETES is larger than 70 nm. When the ETES is reduced down to 50 nm, a new resonance peak appears at about 560 nm. This new resonance peak becomes more distinct due to strong coupling in ultra-small plasmonic gaps when the ETES is further reduced to less than 30 nm. As the ETES is decreased, the linewidth and magnitude of the resonances become sharper and larger. In addition, another resonance peak located at ~ 700 nm also redshifts with decreased ETES. A redshift of about 60 nm is observed when the ETES is tuned from 90 nm (peak at 680 nm) to 10 nm (peak at 740 nm) with an obvious increase of intensity. It is worth mentioning that the sudden intensity drop of the spectrum for ETES = 10 nm is due to fabrication imperfections since it is extremely difficult to precisely control the gap size within such a trivial range. For the resonances located at around 900 nm, similar increasing intensity and redshift of peak positions with decreasing ETES can also be clearly observed. Reflected intensity of the peak increases because the impedance mismatch increases with larger wavelengths in the infrared range.

The observed two reflectance minima (indicated by blue arrows) observed in Fig. 3(a) can be accounted for by Wood's anomalies^{39–42} or the Rayleigh cutoff wavelength^{42,43} for a periodic nanoparticle array. The nanoparticle array works as a buffer layer between two different materials: air and the quartz substrate. The dispersion relations of the incident electromagnetic waves with the same frequencies are different due to different refractive indices. Diffraction occurs on both interfaces of the air/particle array and the particle array/substrate and many modes tend to transmit from air into the substrate. However, total conversion of all the diffraction modes from one medium to another is impossible due to impedance mismatch or different dispersion relations of the electromagnetic waves inside different materials, thus some diffraction modes will disappear during the conversion process and be confined on the interface in the form of surface waves. Those missing diffraction modes are represented as narrow reflection minima in the reflectance spectrum.

Fig. 3(b) plots the measured transmittance as a function of the wavelength. The brown arrow points out the dip corresponding to

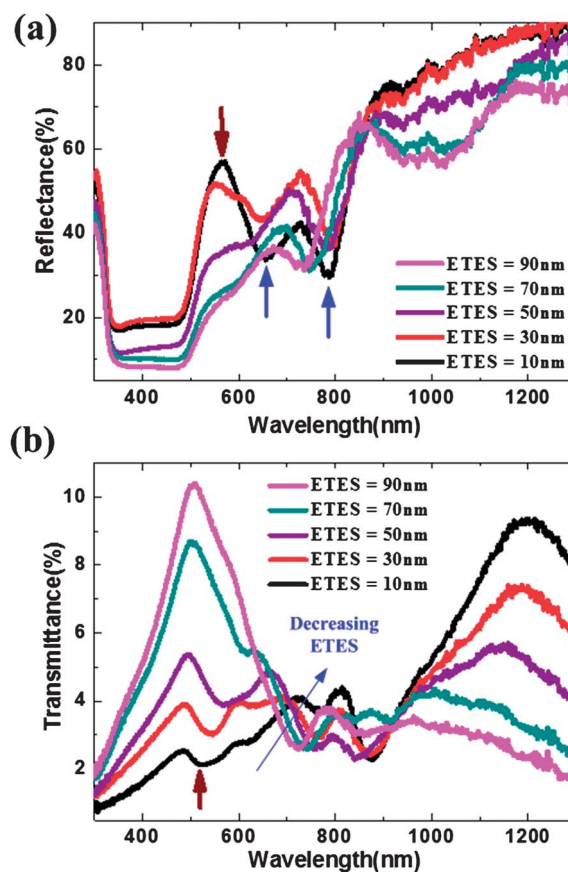


Fig. 3 Measured reflectance (a) and transmittance (b) spectra for plasmonic arrays consisting of diamond-circle shaped lattices with different ETES.

the peak observed in the reflectance spectrum for ETES = 10 nm. A relatively low intensity (less than 10%) is due to the thick metal film used in this work. One can also observe redshift of the resonance located between 700 and 800 nm with decreasing ETES because of larger particle sizes and smaller gaps.⁴⁴

To further explore the underlying physics of the field enhancement associated with ultrascale gaps, FDTD simulations were carried out. Fig. 4 shows the example for ETES = 30 nm with the measured reflectance for comparison. Overall, qualitative agreement is observed between the experimental and simulation results. However, the simulated spectrum presents slight differences with smaller spectral widths (sharper peaks and dips). This divergence is mainly attributed to shape tolerance and the refractive index differences between the simulation and experiment and the convergence of the numerical iteration process in the simulation software. Another important factor resulting in

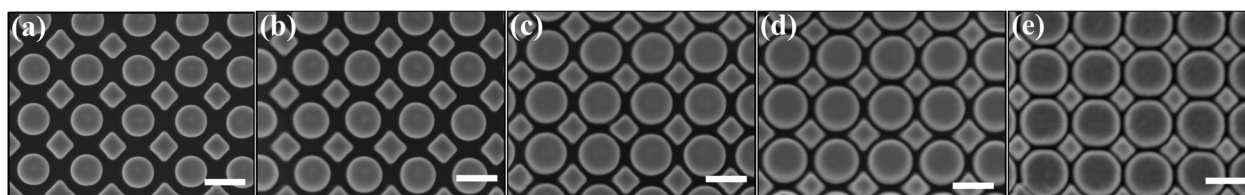


Fig. 2 SEM images showing decreasing ETES from 90 nm (a) to 10 nm (e) for the diamond-circle shaped lattices. All scale bars are 500 nm.

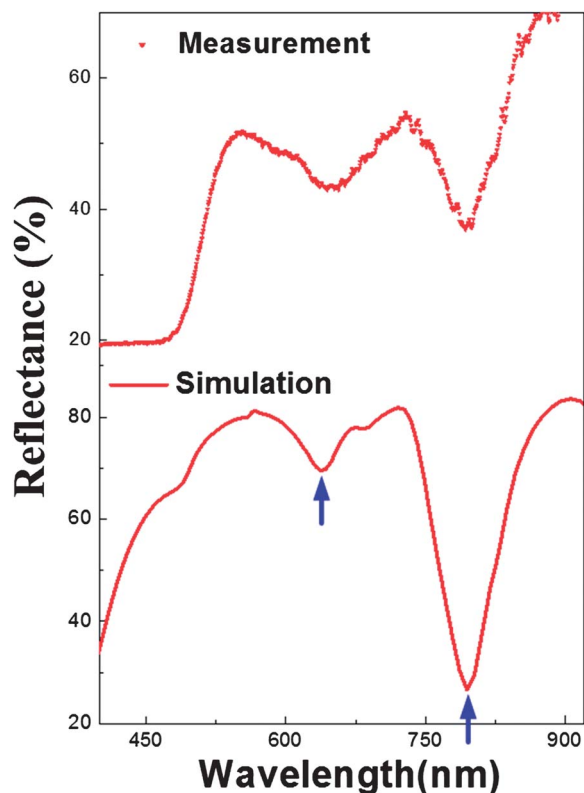


Fig. 4 Measured and FDTD-calculated reflectance of the diamond-circle lattice with ETES = 30 nm.

the slight divergence observed in the simulations and measurements is the rough surface of the real sample for testing caused by material redeposition during FIB milling. We further calculated electric field distributions at two representative positions in Fig. 4 (reflectance minima: 642 nm and 794 nm, indicated by the blue arrows), as shown in Fig. 5. Strong confinement of light inside the cavities can be observed. Reflection dips indicate either transmission or incident energy confinement inside the plasmonic gaps. For our case, the transmission was expected to be less than 10% (as shown in Fig. 3(b)) due to a relatively thick metal film and ultrasmall gap width. Thus the surface energy confinement contributes dominantly to the low energy of the dips shown in the reflectance. The intensity difference indicates the capability for energy confinement of the plasmonic cavities on different surface modes. Competition is expected between the coupling from surface waves into cavity modes staying on the surface and surface waves coupling back to propagating modes leaving the surface as secondary reflections or back scattering. As we can see from Fig. 5, both electric fields are confined as cavity modes inside the ring gaps with an intensity difference corresponding to the prominent and secondary surface wave modes. As expected, the field distribution around 642 nm presents less field intensity as compared to the case of 794 nm, indicating less energy penetration into the plasmonic nanostructures. This is likely to be caused by the preferable coupling from surface modes into propagating modes over confined cavity modes. On the other hand, the field distribution at 794 nm shows a strong intensity as evidence of the strong energy confinement inside the cavities.

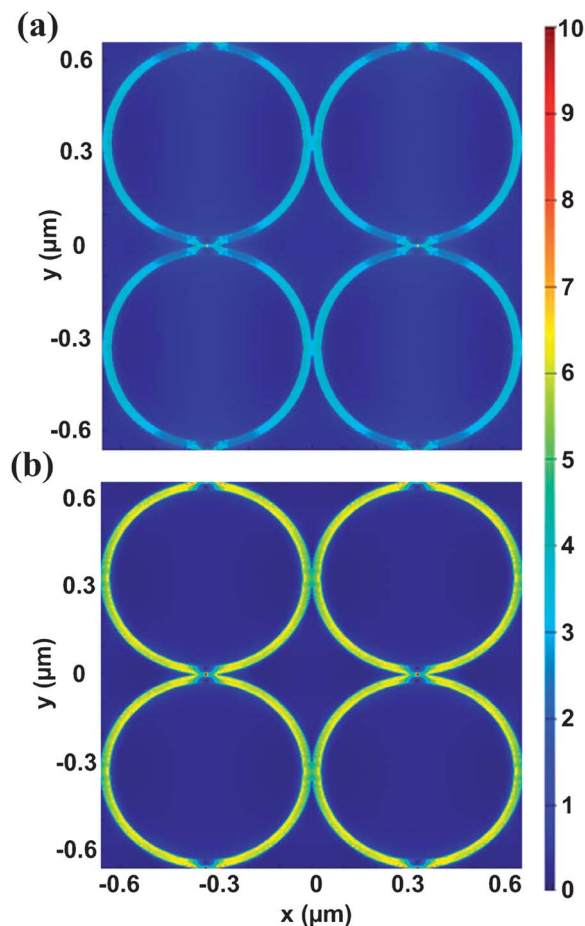


Fig. 5 Calculated electric field distribution at reflectance dips as indicated by blue arrows (in Fig. 4) for the diamond-circle lattice with ETES = 30 nm. (a) 642 nm and (b) 794 nm.

Conclusions

In summary, we have demonstrated a direct and accurate patterning method to achieve plasmonic nanostructures with ultrasmall gaps using the FIB technique. By realigning ring arrays and controlling the overlapping areas, one can fabricate dense plasmonic arrays with varying sizes, shapes and pitches. We have also investigated the tunability of the optical response with different ETES. Plasmon-enhanced reflectance has been observed with ultrasmall ETES due to strong plasmon coupling. Significant field enhancement in ultrasmall gaps is potentially useful for designing complex metamaterials with desired optical responses and specific functions. This high resolution patterning technique can be applied to different geometries with various lattice shapes in a wide range of metallic materials.

Acknowledgements

This work was supported by NEU internal funding XNB201302 and Natural Science Foundation of Hebei Province under grants no. A2013501049 and F2012501023. H. Liu gratefully acknowledges the National Natural Science Foundation of China (grant no. 61007005).

Notes and references

- 1 T. W. Ebbesen, H. J. Lezec, H. F. Ghaemi, T. Thio and P. A. Wolff, *Nature*, 1998, **391**, 667.
- 2 J. B. Pendry, *Phys. Rev. Lett.*, 2000, **85**, 3966.
- 3 J. B. Pendry, D. Schurig and D. R. Smith, *Science*, 2006, **312**, 1780.
- 4 W. Cai, U. K. Chettiar, A. V. Kildishev and V. M. Shalaev, *Nat. Photonics*, 2007, **1**, 224.
- 5 N. Fang, H. Lee, C. Sun and X. Zhang, *Science*, 2005, **308**, 534.
- 6 Z. Liu, S. Durant, H. Lee, Y. Pikus, N. Fang, Y. Xiong, C. Sun and X. Zhang, *Nano Lett.*, 2007, **7**, 403.
- 7 L. Yin, V. K. Vlasko-Vlasov, J. Pearson, J. M. Hiller, J. Hua, U. Welp, D. E. Brown and C. W. Kimball, *Nano Lett.*, 2005, **5**, 1399.
- 8 S. I. Bozhevolnyi, J. Erland, K. Leosson, P. M. W. Skovgaard and J. M. Hvam, *Phys. Rev. Lett.*, 2001, **86**, 3008.
- 9 J. N. Anker, W. P. Hall, O. Lyandres, N. C. Shah, J. Zhao and R. P. Van Duyne, *Nat. Mater.*, 2008, **7**, 442.
- 10 A. V. Kabashin, P. Evans, S. Pastkovsky, W. Hendren, G. A. Wurtz, R. Atkinson, R. Pollard, V. A. Podolskiy and A. V. Zayats, *Nat. Mater.*, 2009, **8**, 867.
- 11 R. Bardhan, N. K. Grady, T. Ali and N. J. Halas, *ACS Nano*, 2010, **4**, 6169.
- 12 S. Mukherjee, H. Sobhani, J. B. Lassiter, R. Bardhan, P. Nordlander and N. J. Halas, *Nano Lett.*, 2010, **10**, 2694.
- 13 J. Aizpurua, P. Hanarp, D. S. Sutherland, M. Käll, G. W. Bryant and F. J. García de Abajo, *Phys. Rev. Lett.*, 2003, **90**, 057401.
- 14 P. Nordlander, *ACS Nano*, 2009, **3**, 488.
- 15 A. W. Clark and J. M. Cooper, *Adv. Mater.*, 2010, **22**, 4025.
- 16 G. Y. Si, Y. H. Zhao, H. Liu, S. L. Teo, M. S. Zhang, T. J. Huang, A. J. Danner and J. H. Teng, *Appl. Phys. Lett.*, 2011, **99**, 033105.
- 17 Y. J. Liu, G. Y. Si, E. S. P. Leong, N. Xiang, A. J. Danner and J. H. Teng, *Adv. Mater.*, 2012, **24**, OP131.
- 18 Y. J. Liu, G. Y. Si, E. S. P. Leong, B. Wang, A. J. Danner, X. C. Yuan and J. H. Teng, *Appl. Phys. A: Mater. Sci. Process.*, 2012, **107**, 49.
- 19 H. Wang, D. W. Brandl, F. Le, P. Nordlander and N. J. Halas, *Nano Lett.*, 2006, **6**, 827.
- 20 I. Zorić, E. M. Larsson, B. Kasemo and C. Langhammer, *Adv. Mater.*, 2010, **22**, 4628.
- 21 Y. J. Liu, Q. Hao, J. S. T. Smalley, J. Liou, I. C. Khoo and T. J. Huang, *Appl. Phys. Lett.*, 2010, **97**, 091101.
- 22 Y. J. Liu, W. W. Loh, E. S. P. Leong, T. S. Kustandi, X. W. Sun and J. H. Teng, *Nanotechnology*, 2012, **23**, 465302.
- 23 Y. J. Liu, Q. Hao, J. S. T. Smalley, J. Liou, I. C. Khoo and T. J. Huang, *Appl. Phys. Lett.*, 2010, **97**, 091101.
- 24 J. A. Dionne, K. Diest, L. A. Sweatlock and H. A. Atwater, *Nano Lett.*, 2009, **9**, 897.
- 25 V. Malyarchuk, F. Hua, N. H. Mack, V. T. Velaasquez, J. O. White, R. G. Nuzzo and J. A. Rogers, *Opt. Express*, 2005, **13**, 5669.
- 26 Y. Shen, X. Chen, Z. Dou, N. P. Johnson, Z. Zhou, X. Wang and C. Jin, *Nanoscale*, 2012, **4**, 5576.
- 27 B. Gallinet and O. J. F. Martin, *ACS Nano*, 2011, **5**, 8999.
- 28 L. Tong, H. Wei, S. Zhang, Z. Li and H. Xu, *Phys. Chem. Chem. Phys.*, 2013, **15**, 4100.
- 29 S. Zhang, Y. Park, Y. Liu, T. Zentgraf and X. Zhang, *Opt. Express*, 2010, **18**, 6048.
- 30 A. M. Kern and O. J. F. Martin, *Nano Lett.*, 2011, **11**, 482.
- 31 W. Zhang, L. Huang, C. Santschi and O. J. F. Martin, *Nano Lett.*, 2010, **10**, 1006.
- 32 H. Liu, N. Wang, Y. Liu, Y. Zhao and X. Wu, *Opt. Lett.*, 2011, **36**, 385.
- 33 A. Polyakov, K. F. Thompson, S. D. Dhuey, D. L. Olynick, S. Cabrini, P. J. Schuck and H. A. Padmore, *Sci. Rep.*, 2012, **2**, 933.
- 34 M. G. Nielsen, D. K. Gramotnev, A. Pors, O. Albrechtsen and S. I. Bozhevolnyi, *Opt. Express*, 2011, **19**, 19310.
- 35 G. Si, A. J. Danner, S. L. Teo, E. J. Teo, J. Teng and A. A. Bettiol, *J. Vac. Sci. Technol., B: Microelectron. Nanometer Struct.–Process., Meas., Phenom.*, 2011, **29**, 021205.
- 36 Lumerical, <http://www.lumerical.com>.
- 37 P. B. Johnson and R. W. Christy, *Phys. Rev. B: Solid State*, 1972, **6**, 4370.
- 38 N. Liu, T. Weiss, M. Mesch, L. Langguth, U. Eigenthaler, M. Hirscher, C. Sönnichsen and H. Giessen, *Nano Lett.*, 2010, **10**, 1103.
- 39 R. W. Wood, *Philos. Mag.*, 1902, **4**, 396.
- 40 R. W. Wood, *Philos. Mag.*, 1912, **23**, 310.
- 41 R. W. Wood, *Phys. Rev.*, 1935, **48**, 928.
- 42 J. E. Stewart and W. S. Gallaway, *Appl. Opt.*, 1962, **1**, 421.
- 43 M. Sarrazin, J. Vigneron and J. Vigoureux, *Phys. Rev. B: Condens. Matter*, 2003, **67**, 085415.
- 44 S. K. Ghosh and T. Pal, *Chem. Rev.*, 2007, **107**, 4797.